arXiv:2205.00579v1 [cs.LG] 1 May 2022

Data-driven control of spatiotemporal chaos with reduced-order neural ODE-based models and reinforcement learning

Kevin Zeng, Alec J. Linot, and Michael D. Graham*

Department of Chemical and Biological Engineering,

University of Wisconsin-Madison, Madison WI 53706, USA

(Dated: May 3, 2022)

Abstract

Deep reinforcement learning (RL) is a data-driven method capable of discovering complex control strategies for high-dimensional systems, making it promising for flow control applications. In particular, the present work is motivated by the goal of reducing energy dissipation in turbulent flows, and the example considered is the spatiotemporally chaotic dynamics of the Kuramoto-Sivashinsky equation (KSE). A major challenge associated with RL is that substantial training data must be generated by repeatedly interacting with the target system, making it costly when the system is computationally or experimentally expensive. We mitigate this challenge in a data-driven manner by combining dimensionality reduction via an autoencoder with a neural ODE framework to obtain a low-dimensional dynamical model from just a limited data set. We substitute this data-driven reduced-order model (ROM) in place of the true system during RL training to efficiently estimate the optimal policy, which can then be deployed on the true system. For the KSE actuated with localized forcing ("jets") at four locations, we demonstrate that we are able to learn a ROM that accurately captures the actuated dynamics as well as the underlying natural dynamics just from snapshots of the KSE experiencing random actuations. Using this ROM and a control objective of minimizing dissipation and power cost, we extract a control policy from it using deep RL. We show that the ROM-based control strategy translates well to the true KSE and highlight that the RL agent discovers and stabilizes an underlying forced equilibrium solution of the KSE system. We show that this forced equilibrium captured in the ROM and discovered through RL is related to an existing known equilibrium solution of the natural KSE.

* Email: mdgraham@wisc.edu

I. INTRODUCTION

In recent years, deep reinforcement learning (RL), a data-driven model-free control method, has achieved recognition for its ability to learn and discover complex control strategies for high-dimensional systems. Many of its milestone achievements involve defeating the best professional players in complex games such as GO [1], DOTA II [2], and Starcraft II [3], as well as the leading GO, Chess, and Shogi engines [4]. The successes of RL in these complex, nontrivial, and high-dimensional systems has made its application towards control of high-dimensional chaotic dynamical systems, such as turbulent flows, extremely promising. Deep RL has recently been demonstrated to be able to discover strategies in flow systems that exhibit nonchaotic dynamics such as reducing the drag in flow over bluff bodies [5–9] and decreasing convection amplitude in Rayleigh-Benard systems [10]. Using the Kuramoto-Sivashinsky equation (KSE) as an example, Bucci et al. [11] demonstrated that RL is able to direct a system with natural chaotic dynamics to a given (i.e. previously known) equilibrium solution of the system. In another study of the KSE in a chaotic parameter regime, the present authors [12] demonstrated that an RL policy whose aim is to minimize dissipation is able to discover and stabilize a nontrivial underlying equilibrium solution with low dissipation, even when no such information of its existence is given. The aim of the present work is to combine RL with data-driven reduced-order dynamical models for the purpose of control of spatiotemporal dynamics, as a step toward the goal of reducing energy dissipation in turbulent flows.

Despite all of the successes of deep RL, a major challenge is that it suffers from poor sampling complexity. For example, recent work by Du et al. [13] showed that even if the optimal control policy could be perfectly represented by a linear function, the reinforcement learning agent still requires an exponential number of trajectories to find a near-optimal policy. Furthermore, the overall practical problem is further exacerbated by the temporal credit assignment problem, which is the difficulty in parsing out what actions in a long series of actions actually contributed to the end result–often bottlenecking RL algorithms attempting to train large models with millions of weights in application [14].

In practice this issue is often addressed by simply brute-force generating an extraordinary amount of interaction data from the target system for training. For example, to achieve the

previously mentioned accolades, over 11,000+ years of DOTA II gameplay [2], 4.9 million self-play games of GO [1], and 200 years of Starcraft II gameplay [3] was required. In the realm of fluid control, even to learn a two parameter control scheme for reducing drag in an LES bluff-body simulation required over 3 weeks of training and simulation time [6]. The default solution of simply generating more data can quickly make deep RL a prohibitively costly solution when the target flow system is computationally (e.g. via direct numerical simulations) or experimentally (e.g. via wind tunnel tests) expensive to realize.

Despite these challenges, there are growing efforts toward developing more data-efficient learning algorithms and work-around techniques. These efforts can be broadly categorized into three classes: advanced RL algorithms, true off-policy RL, and model-based RL. The first class, advanced RL algorithms, is comprised of methods that either build upon existing established algorithms with advanced architectures and formulations or by building in domain knowledge to improve training stability and data efficiency at the cost of increasing implementation and training complexity.

The second class, true off-policy RL, is comprised of methods that reformulate the typical semisupervised RL problem into a supervised learning problem in order to extract control strategies from an existing limited data set of transitions. However, these methods are still in the very early stages of development and it is still unclear how well they perform and generalize in complex systems.

The last class, model-based RL, are methods that utilize a model of the target environment. These methods are advantageous in that they can leverage the existing vast classical modeling principles as well as the newly emerging deep learning techniques. As a result, model construction, implementation, and degree of data-drivenness vary widely from method to method. For example, Nagabandi et al. [15] introduced the Model-Based+Model-Free method, which utilizes a system model and an MPC controller to initialize the RL agent's weights. Towards more data-driven approaches, Wahlstrom et al. [16] introduced Deep Dynamical Models, which uses an autoencoder to learn a reduced-order representation of the observation data and a feedforward neural network to learn a discrete time stepping model in said reduced-order representation to control an inverted pendulum from pixel inputs. Similarly, Watter et al. [17] also utilized autoencoders and feedforward neural networks to learn a local linear dynamical representation of the pendulum problem. Feinberg et al. [18] utilized

models to generate short "imagined" trajectories at each training step to better estimate the value functions. This so-called "Dyna"-style of model-based RL [19] has been recently applied in control of spatiotemporally chaotic systems by Liu et al. [20] who demonstrated with autoencoded recurrent network models containing hardcoded boundary conditions and soft conservation constraints that the number of real interactions needed with the target system to achieve control could be greatly reduced. Finally, Ha and Schmidhuber [14] introduced recurrent world models, which model the control system of interest with mixture density networks and recurrent neural networks. In this method, the authors use a data-driven model in place of the real environment during RL training to estimate a control policy for driving a 2D car and playing DOOM. We will refer to this style of utilizing a data-driven model as a surrogate training ground as "model-based RL".

The learning process of the above defined model-based RL parallels the classic control design philosophy [21] which is: 1) create a model for control, 2) design a control policy based on the model, and 3) simulate based on a high-fidelity model and repeat if needed. In parallel to these principles, we seek to: 1) *learn* a model – specifically a reduced-order, but still highly accurate model – for control from data, 2) *learn* a control policy based on the model with RL, and 3) validate based on a high-fidelity model.

A key aspect of this approach is the development of an efficient reduced-order model of the process, which we will consider to be completely governed by a state space representation

$$\frac{ds}{dt} = f(s, a), \tag{1}$$

or its discrete-time version

$$s_{t+\tau} = F(s_t, a_t), \tag{2}$$

where $s \in \mathbb{R}^d$ is the state of the system and $a \in \mathbb{R}^{d_a}$ a time-dependent actuation. Our focus will be the continuous-time case Eq. 1, where we will seek a reduced-order representation

$$\frac{dh}{dt} = f(h, a), \tag{3}$$

where $h \in \mathbb{R}^{d_h}$ and $d_h \ll d$. Before describing our specific approach, we briefly review other methods for developing dynamic models from data. A more detailed discussion is given in [22].

If the governing equations of the process are known, one approach is simply to use a direct simulation without any model reduction. Here of course none of the efficiency gains enabled

by reducing the dimension of the model are realized. A traditional approach to reducing the dimension of these problems is the Galerkin projection method [23] and other variants like nonlinear Galerkin [24–26] or posprocessing Galerkin [27], which have higher accuracy than the traditional Galerkin approach for given number of unknowns. Additionally, such approaches can be improved by adding data-driven information. For example, Wan et al. [28] approximated the unresolved dynamics in nonlinear Galerkin with an LSTM. The concept of combining first-principles and data-driven models is a widely studied one (see e.g. "physics-informed neural networks" [29]).

In the present work, however, our focus is data-driven models. The classical approach is to seek a linear discrete-time model; a specific example of this approach, which has seen wide use recently even for nonlinear systems, is dynamic mode decomposition (DMD)[30]. We describe and implement an adaption of DMD to closed loop control, known as DMDc, in Section IIIB. As a linear state space model, at long times, trajectories predicted by DMD always evolve toward a fixed point or a quasiperiodic orbit with a discrete set of frequencies, so it cannot faithfully characterize chaotic dynamics, which is our interest here. In principle, for all nonlinear systems there does exist a linear, albeit infinite-dimensional, operator called the *Koopman* operator that describes the evolution of arbitrary observables [31, 32]. We choose not to take this approach because our aim is to reduce the dimension of our model. In any case, effective methods for approximation of chaotic long-time dynamics with data-driven Koopman operator approximations remain elusive.

With the increasing power of neural network representations, nonlinear data-driven modeling methods have received substantial recent attention. Two popular methods include recurrent NN (RNN) [33, 34] and reservoir computing [35, 36]. These approaches are similar in that a hidden or reservoir state r_t is used along with the current state s_t to predict a future hidden or reservoir state $r_{t+\tau}$. Then a function is used to predict the new state $s_{t+\tau}$ from the hidden state. The two approaches are different in how these functions are approximated. In reservoir computing the functions for evolving the reservoir are chosen a priori, and the mapping back to $s_{t+\tau}$ is learned. In RNNs, specific neural networks are trained to learn all of the functions – two examples are LSTMs [34] and gated recurrent units [37]. Vlachas et al. [38] shows that both these methods perform well at predicting chaotic dynamics. However, because they involve hidden variables, these approaches do not reduce the dimension of

the system, but rather increase it: i.e. they do not determine $s_{t+\tau}$ from s_t alone, but rather also use past history stored in r_t to make predictions.

A more direct approach to learning dynamical models is to learn the right-hand side (RHS) of Eq. 1 or Eq. 2 from data. One way to do this, at least for low-dimensional systems, is using the "Sparse Identification of Nonlinear Dynamics " (SINDy) approach [39]. In this method a dictionary of candidate nonlinear functions are selected to approximate f in Eq. 1. Then, by using sparse regression, the dominant terms are identified and kept. Alternately, one could simply represent f with a neural network [40]. If one does not have time-derivative data or estimates, then the neural ODE approach [22, 41] can be used.

Now we turn to the issue of dimension reduction. The dynamics of formally infinite-dimensional partial differential equations describing dissipative flow systems are known to collapse onto a finite-dimensional invariant manifold [42]–a so-called "inertial manifold". In past works, it was shown that one can capture a high-dimensional system's dynamics on this lower-dimensional manifold by using a combination of autoencoders, to identify the manifold coordinates, and Neural ODEs (NODE) [41], to model the dynamics on the manifold in discrete time [43] or continuous time [22].

Our aim is to adapt this data-driven, low-dimensional model framework as a data-efficient surrogate training grounds for model-based RL. Once training is complete, this ROM-based policy is then deployed to the real system for assessment or further fine tuning. We refer to our method as *Data-driven Manifold Dynamics for Reinforcement Learning*, or DManD-RL for short.

Unlike the previous implementations of data-driven models in model-based RL [14, 16, 17], which model the evolution of the controlled system in fixed discrete time steps, our method models the vector field of the dynamics on the manifold in the presence of control inputs using neural ODEs [41]. The choice of using neural ODEs has several benefits: 1) it allows one to utilize the vast and already present array of integration schemes for time-stepping, 2) it allows one to train the model from data collected from variable time step sizes as well as make variable time step predictions, which grants one the ability to adjust the transition time step in RL without resorting to recollecting new data and training a new dynamics model, 3) it is a natural formulation for the modeling of the dynamics of our physical flow systems. We highlight that this framework is not limited to fixed time intervals, can utilize unevenly

and/or widely spaced data in time, respects the Markovian nature of the dynamics of the systems we are interested in capturing, and respects the Markov environment assumption that underlies RL theory [19], unlike other common data-driven approaches such as recurrent neural networks [33, 34] and reservoir computing [35, 36]. Finally, we do not impose that the underlying relationship between the control input and the dynamics is affine in control (i.e. that $\frac{ds}{dt} = f(s) + g(s)a$ where s is the state and a is the control input), as some past works have done [17]. This is advantageous for application towards complex flow control systems of practical interest as many, such as aircraft [44] and underwater vehicles [45], do not have relationships with this affine structure.

The remainder of this paper is structured as follows: In Section II we introduce the Kuramoto-Sivashinsky equation, a proxy system for turbulent flows that displays rich spatiotemporal chaos, and the control objective which serves as a drag reduction analogue. We conclude this section with an outline of our ROM-based RL framework. In Section III we examine the performance of our learned reduced-order model, the control strategy extracted from the model using RL, and the dynamical systems relevancy of the strategy. In Section IV we conclude our findings and discuss applications to more complex systems.

II. FORMULATION

A. Kuramoto-Sivashinsky Equation

The Kuramoto Sivashinsky Equation (KSE) is given by,

$$\frac{\partial v}{\partial t} = -v\frac{\partial v}{\partial x} - \frac{\partial^2 v}{\partial x^2} - \frac{\partial^4 v}{\partial x^4} + f(x,t). \tag{4}$$

Here f is a spatio-temporal forcing term that will be used for control actuation. We consider the KSE in a domain of length $L = 22$ with periodic boundary conditions as this is a dynamically well characterized system [46]. The uncontrolled KSE, $f = 0$, exhibits rich dynamics and spatio-temporal chaos, which has made it a common toy problem and proxy system for the Navier-Stokes Equations. Spatially localized control is implemented in the KSE with $N = 4$ equally spaced Gaussian "jets" located at $X \in \{0, L/4, 2L/4, 3L/4\}$ as done by Bucci et al. [11] and Zeng and Graham [12], where $a_i(t) \in [-1, 1]$ is the control

signal output by the RL control agent,

$$f(x,t) = \sum_{i=1}^{4} \frac{a_i(t)}{\sqrt{2\pi}\sigma_s} \exp\left(-\frac{(x-X_i)^2}{2\sigma_s^2}\right). \tag{5}$$

The system is time evolved with a time step of $\Delta t = 0.05$ using the same numerical method and code as Bucci et al. [11] with a third-order semi-implicit Runge-Kutta scheme, which evolves the linear second and fourth order terms with an implicit scheme and the nonlinear convective and forcing terms with an explicit scheme. Spatial discretization is performed with Fourier collocation on a mesh of 64 evenly spaced points and in our formulation the state vector u consists of the solution values at the collocation points. To serve as an analogue to energy-saving flow control problems, we are interested in the minimization of the dissipation, D, and total power input, P_f required to power the system and jets of the KSE system, which are described by $D = \langle(\frac{\partial^2 u}{\partial x^2})^2\rangle$ and $P_f = \langle(\frac{\partial u}{\partial x})^2\rangle + \langle uf\rangle$, respectively. Here $\langle\cdot\rangle$ is the spatial average.

B. Background and Method Formulation

At its core, deep RL is a cyclic learning process with two main components: the RL agent and the environment. The agent is the embodiment of the control policy and generally a neural network, while the environment is the target system for control. During each cycle, the agent makes a state observation of the system, s_t, and outputs an action, a_t. The impact of this action on the environment is then quantified by a scalar quantity, r_t, which is defined by the control objective. During training, the agent attempts to learn the mapping between s_t and a_t that maximizes the cumulative long time reward and updates accordingly each cycle. This learning cycle is shown in Fig. 1.

Deep RL's poor sampling complexity makes this cyclic process costly or even intractable for learning control strategies when simulations or experiments of the environment are expensive to realize. We aim to circumvent this issue in a completely data-driven manner by training the RL agent with a surrogate reduced-order model (ROM) of the target system. Our method can be divided into five steps: 1) obtain ROM training data 2) learn a reduced-order embedding coordinate transformation using an autoencoder 3) learn the RHS of the controlled system's dynamics in the reduced-order coordinates using Neural ODEs,

4) extract a control policy from this ROM using deep RL, 5) deploy and assess the control strategy in the real system. An outline of this process is presented in Fig. 2.

Step 1: Training Data Collection: We obtain our training data for our data-driven model by observing actuated trajectories of the target system. As we assume there is neither a model nor control strategy available at this stage, the actuations applied are randomly sampled from a uniform distribution of the available range of control inputs. The observed series of states, s_t, applied actions, a_t, at time t, and the resulting state after τ time units, $s_{t+\tau}$ are saved as transition snapshots $[s_t, a_t, s_{t+\tau}]$ for ROM training. In our demonstration with the KSE, we take the state observable to be the solution of the KSE at time t, $s_t = u(t)$, and the coinciding control signals to the jet actuations to be the action, $a_t = a(t)$ (where $a_i(t)$ is the signal to the ith jet).

Step 2: Learning the Manifold Coordinate System: We utilize undercomplete neural network autoencoders [47] to learn the coordinate transformation to and from the lower-dimensional manifold of the actuated dynamics of our system. Undercomplete autoencoders are hourglass-shaped neural networks that are composed of two subnetworks, the encoder and decoder, are connected by a size-limiting bottleneck layer that explicitly restricts the number of degrees of freedom that the input data must be represented by. This structure forces the encoder to learn to compress the input data to a representation that fits through the bottleneck and the decoder to learn to reconstruct the original input from the compressed representation while minimizing information loss across the network. In our work, the encoder, $h_t = \chi(s_t; \theta_E)$, is tasked with learning the mapping from the full-state representation, $s_t \in \mathbb{R}^{d_s}$, to the manifold representation, $h_t \in \mathbb{R}^{d_h}$, and is parameterized by weights θ_E. Importantly, $d_h \ll d_s$, such that the bottleneck layer explicitly restricts the number of degrees of freedom representing our data, as our objective is to learn a reduced-order manifold representation. The decoder, $\hat{s}_t = \tilde{\chi}(h_t; \theta_D)$, is tasked with learning the mapping from the manifold representation to the full-state representation and is parameterized by weights θ_D. The autoencoder is trained to minimize the mean squared reconstruction loss (MSE) $\mathcal{L}_{AE} = \langle ||s_t - \hat{s}_t||^2 \rangle$ where $\hat{s}_t = \tilde{\chi}(\chi(s_t))$ using the snapshots of state data obtained from the previous step and $\langle \cdot \rangle$ is the average over a training batch. In our example with the KSE we also perform an intermediary change of basis from the observed state s_t to its projection onto the Principal Component Analysis basis (computed from the training data)

prior to input to $\chi(s_t;\theta_E)$ and a return to the full space post output from $\tilde{\chi}(h_t;\theta_D)$ as we found this to be an effective intermediate basis in learning. We identify the dimension of the finite dimensional manifold, $d_{\mathcal{M}}$, by tracking the MSE performance of the autoencoders as we vary d_h, [22, 43].

Step 3: Learning the Actuated Dynamics along the Manifold: We next develop a neural-ODE (NODE) model of the dynamics in the manifold coordinates h by learning the RHS (vector field) of the ODE $\dot{h} = g(h_t, a_t; \theta_M)$, where θ_M denotes the neural-network parameters that are to be determined [41]. To make dynamical forecasts given a manifold state, h_t, and input control action, a_t, the evolution of the manifold state τ time units forward, $h_{t+\tau}$, can be computed for a given $g(h_t, a_t; \theta_M)$ with a standard time-integration algorithm. To train the NODE network, the same dataset generated in step 1, $[s_t, a_t, s_{t+\tau}]$ can used. Because the NODE network's purpose is to model the vector field of the dynamics in the manifold coordinates, we must first converted the training data to $[h_t, a_t, h_{t+\tau}]$ using $\chi(s_t;\theta_E)$. This data set can then be used to train the NODE network to minimize the forecasting loss: $\mathcal{L}_{NODE} = \langle ||h_{t+\tau} - \hat{h}_{t+\tau}||^2 \rangle$ where $\hat{h}_{t+\tau}$ is the forecast made by integrating the NODE with a numerical integrator forward τ time units. In this work we use the Dormand-Prince 45 numerical scheme [48]. The gradient of the loss with respect to the network parameters, θ_M, can be obtained by either performing back-propagation via automatic differentiation through all the steps of the time integration scheme (which can be memory intensive for very large forecasts) or by the adjoint method described by Chen et al. [41]. In this work we opt for the former as we did not encounter memory issues and past works have demonstrated good agreement between both options [22]. We highlight that once training is complete, NODE forecasted trajectories, which are in the manifold coordinates, can be recovered back to the original ambient space, s, at any point using the decoder, $\tilde{\chi}(h_t;\theta_D)$, obtained in step 2.

Step 4: Learning a control strategy from the NODE-ROM with deep RL: We differentiate our DManD-RL method from typical RL with two distinctions. First the RL agent learns by interacting with the learned NODE-ROM, not the true environment. Second, during training the RL agent learns in the manifold coordinate, h, not the observable space, s. We point out that the usual RL nomenclatures for state transitions, s_{t+1} or s', are written here as $h_{t+\tau}$ in the manifold representation and $s_{t+\tau}$ in the ambient representation, to make

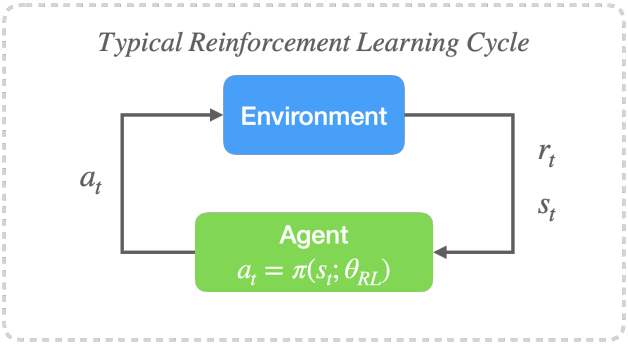

FIG. 1: Typical reinforcement learning cycle.

explicit the fact that the time interval τ is in fact a parameter of the system. To train the RL agent, the NODE-ROM is first initialized with an encoded initial condition. The agent learns by interacting only with the NODE-ROM: given a state in the manifold representation, h_t, the agent attempts to map it to the optimal control action. This action is then passed back to the NODE-ROM and the evolution in h subject to the prescribed actions is obtained by integrating the NODE-ROM forward in time. In this work we aim to lower the total power consumption $D + P_f$ of the KSE dynamics, so we define the immediate reward for the RL algorithm as $r_t = -(D(t)+P_f(t))$. The algorithm seeks to maximize the long time discounted cumulative reward $R_t = \sum_{l=0}^{\infty} \gamma^l r_{t+l\tau}$ where $\gamma = 0.99$. The reward return for this manifold state-action pair $([h_t, a_t])$ can be estimated by decoding the resulting manifold trajectory using $\tilde{\chi}(h_t; \theta_D)$ and estimating r_t, which is used to update the agent. The learning cycle then repeats. In this work we utilize the Deep Deterministic Policy Gradient (DDPG) RL method [49], but we emphasize that any general RL method can be used with our framework.

Step 5: Deploying and Validating the DManD-RL Control Strategy: Once RL training within the NODE-ROM is complete, the learned DManD-RL policy can be applied to the true system. As the agent was trained in the reduced manifold space, the encoder obtained in step 2 must be inserted between the environment and agent to map state observations to the manifold representation prior to input to the agent. The DManD-RL policy can then be applied in typical closed-loop fashion. If desired, new additional on-policy data can be collected to further improve the model/agent in an iterative fashion or the agent can even be simply fine-tuned with real-system training.

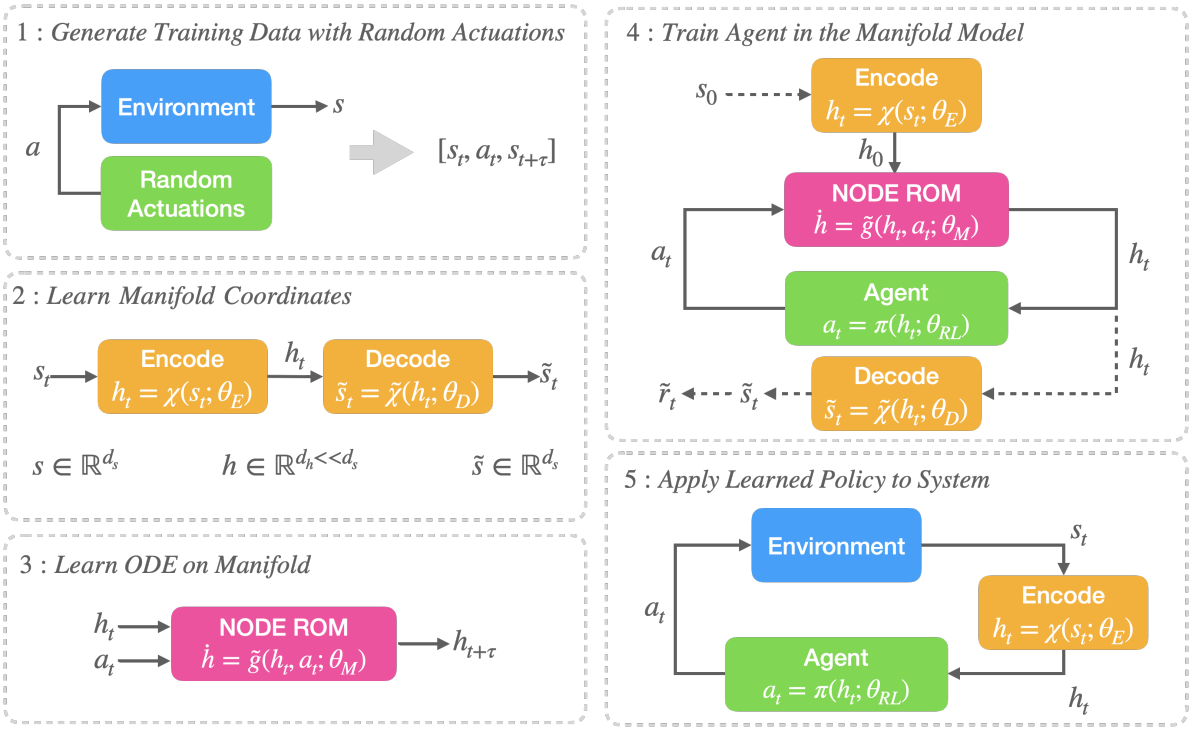

FIG. 2: Procedure for learning a NODE-ROM from data, combining it with RL to approximate a control policy, and deploying the approximate policy back to the true system.

III. RESULTS

A. Neural ODE Model Evaluation

Training data was collected by capturing snapshots of the KSE experiencing jet actuations whose magnitude and direction are randomly sampled from a uniform distribution of the allowable action range described in Section II. We collect 40,000 of these transition snapshots spanning 10,000 time units for our NODE-ROM training, where $\tau = 0.25$ time units. We emphasize here that in this study τ is kept constant for simplicity but in practice τ can vary from snapshot to snapshot. Actuation signals applied during these trajectories and during control are held constant for the duration of τ (i.e. zero-order hold; see Fig. 5a for typical actuation trajectories).

As the autoencoder serves as the mapping function to and from the manifold representation h_t, we need to estimate the number of degrees of freedom in the manifold, d_h, to

accurately capture the dynamics of the system. As d_h is generally not known a priori for complex systems, we empirically estimate it by tracking the reconstruction error as a function of d_h as done by Linot and Graham [22, 43]. In this work our autoencoder networks utilize encoders and decoders each with a hidden layer of size 500 activated by sigmoid functions.

Before considering actuated data, we first apply the autoencoder analysis to the natural unactuated KSE. For the domain size $L = 22$ considered here, the manifold dimension has been determined to be $d_{\mathcal{M}} = 8$ in past studies [43, 50]. This will aid in validating our procedure and give insight into the results with the actuated system. To validate our procedure with the natural KSE, we collect 40,000 snapshots of the KSE where $a_t = 0$, to capture the unactuated KSE dynamics. Shown in Fig. 3a are the mean-squared errors (MSE) of reconstruction for undercomplete autoencoder networks trained on natural, unactuated KSE snapshots for bottleneck layers of varying dimension d_h. We note that as d_h increases from 7 to 8 the MSE exhibits a sharp drop. Here, $d_h = 8$ corresponds to the minimum number of degrees of freedom required to fully represent the manifold in which the natural KSE data lives, which agrees with previous studies [43, 50]. We denote this manifold dimension of $d_h = 8$ as $d_{\mathcal{M}}$. We note that increasing d_h beyond $d_{\mathcal{M}}$ does not significantly improve reconstruction error, indicating that the data can be effectively represented in $d_h = 8$ and additional dimensions are superfluous [43].

Repeating this analysis with the snapshots collected from the randomly actuated KSE to estimate the dimensionality of the actuated dynamics, we observe a similar phenomenon. Shown in Fig. 3b are the mean-squared errors of reconstruction as d_h is changed for undercomplete autoencoders trained with KSE snapshots obtained from trajectories perturbed randomly by the four jet actuators. We note that compared to the Fig. 3a, the sharp drop in MSE is delayed to $d_h = 9$, with a lesser drop at $d_h = 11$.

To dynamically explain this, shown in Fig. 3c is a cartoon of the $d_{\mathcal{M}} = 8$ embedded manifold $\mathcal{M}$ on which the long time dynamics of the unactuated KSE lives, where states that begin off of the manifold are attracted exponentially to it due to dissipation. When actuations are applied, the KSE produces states and trajectories that live off of the natural attractor, effectively giving the manifold "thickness" in additional dimensions, as shown schematically in Fig. 3d. This "thickness" require additional degrees of freedom, i.e. increased $d_{\mathcal{M}}$ from the original system, to accurately capture the dynamics.

To further support this view, shown in Fig. 4 is the power spectral density of the unactuated and actuated data sets $u(t)$ used to train the autoencoders shown in Fig. 3. We note that in the presence of actuations the data exhibits a broadening of the high-wavenumber tail compared to the unactuated data. Physically, this indicates that there are additional high-wavenumber spatial features in the actuated data set, which require additional degrees of freedom to accurately capture. Finally, we highlight in Fig. 3a and Fig. 3b that our autoencoders outperform dimensionality reduction using only Principal Component Analysis in reconstruction error by several orders of magnitude once $d_{\mathcal{M}}$ has been reached.

The autoencoder MSE landscape of the actuated KSE data suggests that a manifold representation of $d_h = 12$ should be sufficient to capture the dynamics of the controlled KSE. Using the $\chi, \tilde{\chi}$ mappings learned by the $d_h = 12$ autoencoder, a NODE network with two hidden layers of size 200, 200 with sigmoid activation was trained to model the actuated dynamics in the $d_h = 12$ manifold. This NODE was trained using the same data used to train the autoencoder by simply converting the collected data of $[s_t, a_t, a_{t+\tau}]$ to $[h_t, a_t, h_{t+\tau}]$ with $h_t = \chi(s_t; \theta_E)$.

To demonstrate the learned NODE-ROM's predictive capability, shown in Fig. 5c and Fig. 5d are two example KSE trajectories experiencing random jet actuation signal sequences visualized in Fig. 5a, Fig. 5b, respectively. We also show in Fig. 5e and Fig. 5f the decoded $d_h = 12$ trajectory forecast by the NODE-ROM beginning from the same initial condition and following the same actuation signal sequence as its ground truth trajectory, Fig. 5c, Fig. 5d, respectively. We note that the forecasted trajectories agree qualitatively with the ground truth for about 20-30 times units or 1-1.5 Lyapunov times of the natural system.

To quantitively compare the ensemble performance of the NODE-ROM and the actuated KSE, an ensemble of 50 actuated forecast/ground truth pairs of trajectories (where the random actuation sequence and initial conditions between each pair are the same) was used to compute the spatial and temporal autocorrelation, shown in Fig. 6a and Fig. 6b, respectively. We note that the NODE-ROM accurately captures the spatial autocorrelation of the actuated KSE, while the temporal autocorrelation exhibits good agreement with a slight temporal dilation. These results indicate that the NODE-ROM is accurately capturing the distribution of features of the actuated KSE in both space and time.

As the NODE-ROM was trained with only transition snapshots experiencing random

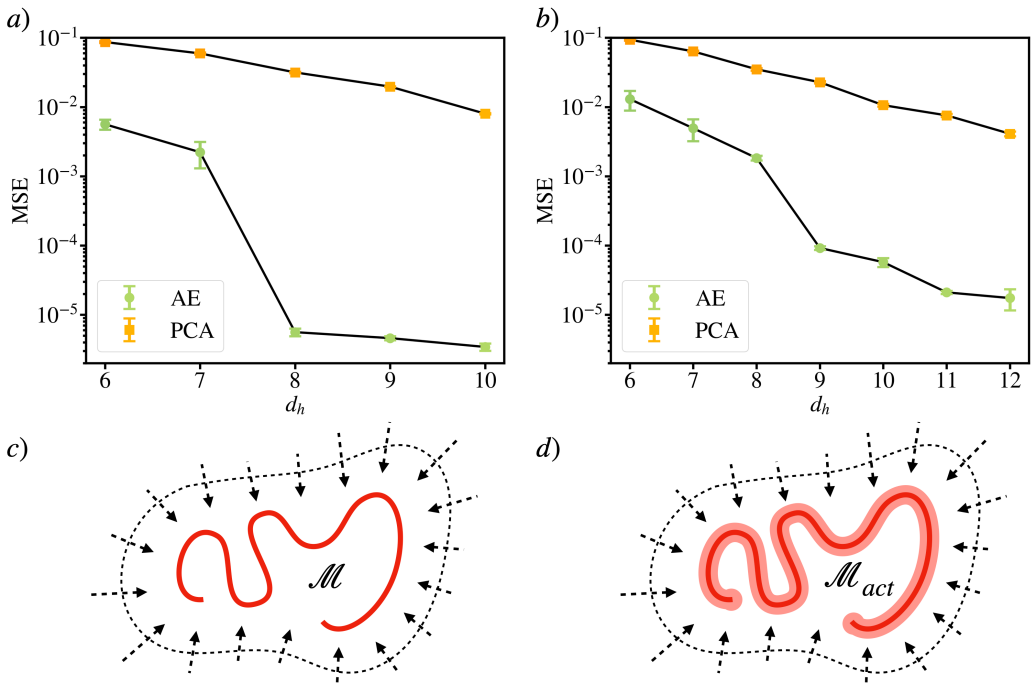

FIG. 3: Mean squared reconstruction error for autoencoders trained on a) unactuated and b) actuated KSE data vs. manifold representation dimension, d_h. Cartoon illustrations of the inertial manifolds in which the data lives on for the c) unactuated and d) actuated system.

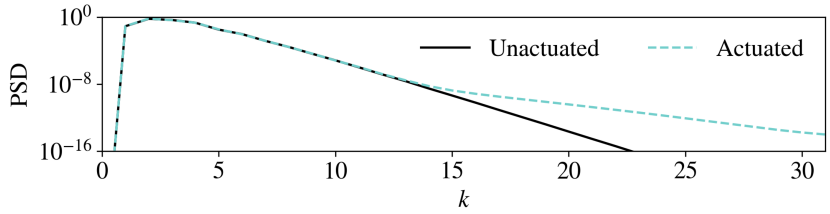

FIG. 4: Power spectral density vs. wavenumber of unactuated and actuated data.

actuations, a natural question is: how well does our model capture the underlying natural dynamics, i.e. with $a_t = 0$? Shown in Fig.7a and Fig.7b are two example natural KSE trajectories where $a_t = 0$. Accompanying the unactuated ground truth trajectories shown in Fig.7a and Fig.7b are the decoded $d_h = 12$ trajectories forecasted by the same NODE-ROM that was trained on actuated data beginning from the same initial conditions and with zero actuation signal input, shown in Fig.7c and 7d, respectively. We note that the forecasted trajectories agree qualitatively with the ground truth for about 1-1.5 Lyapunov times. We

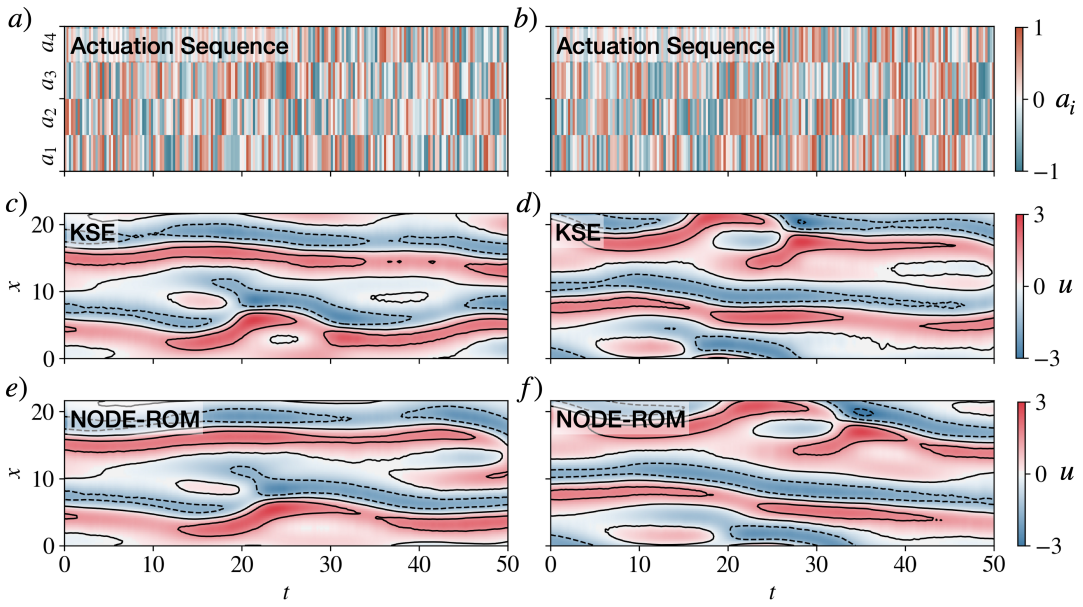

FIG. 5: (a) random actuation sequences $a_i(t)$ (c) ground truth KSE trajectory starting from a random initial conditions following actuation sequences in (a), (e) the decoded NODE-ROM trajectory following actuation sequence (a) and the same initial condition in (c). A second example is shown in (b), (d), and (f), respectively.

again assess the spatial and temporal autocorrelations between an ensemble of 50 pairs of ground truth trajectories and NODE-ROM forecasts, shown in Fig. 6c and 6d, respectively. We note that the ROM matches the spatial autocorrelation of the KSE very well while the temporal autocorrelation reveals that the ROM exhibits a more pronounced but still quantitatively small temporal dilation. We emphasize that despite the training data for the ROMs were obtained from randomly actuated trajectories and that there is no substantial unactuated data, the ROMs still recovers the unactuated dynamics well.

B. Model-Based Control Performance

With this data-driven NODE-ROM, a control agent was trained by interacting only with the NODE-ROM in the manifold space with r_t estimated from the $s = \tilde{\chi}(h; \theta_D)$ decoded state. We set the NODE-ROM model transition time to be $\tau = 0.25$ for all experiments. The control agent was trained with 1000 episodes of 100 time units long (i.e. 400 transitions

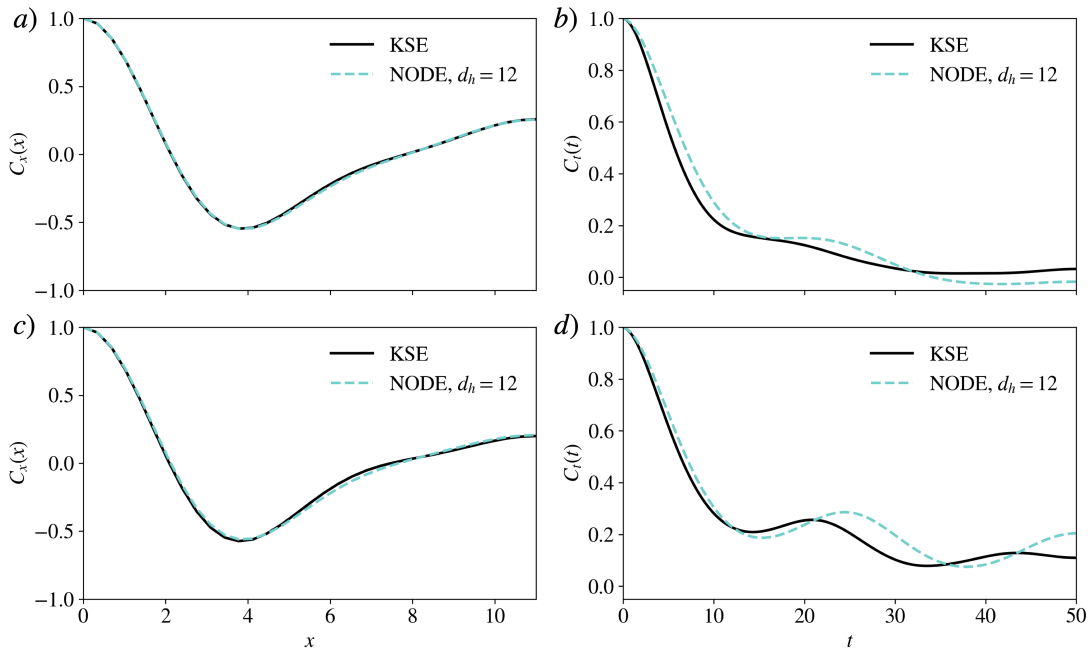

FIG. 6: a) Spatial and b) temporal autocorrelation computed from an ensemble of trajectories experiencing random jet actuations. NODE-ROM ($d_h = 12$) forecasts were produced using the same initial conditions and jet actuation sequences as each respective trajectory produced from the true KSE. c) Spatial and d) temporal autocorrelation computed from an ensemble of trajectories with actuations set to zero. NODE-ROM ($d_h = 12$) forecasts were produced using the same initial conditions as each respective trajectory produced from the true KSE.

per episode), with each episode beginning from a random on-attractor initial condition of the natural, i.e. unforced, KSE. Jet actuations implemented by the control agent, a_t, were maintained constantly from s_t to $s_{t+\tau}$. In this work the DDPG actor and critic networks utilized ReLU activated hidden layers of size 128 and 64, respectively, followed by tanh and linear activations to the outputs of size 4 and 1, respectively.

To assess the performance of our DManD-RL policy, the learned control agent was applied to the NODE-ROM, with an example controlled trajectory shown in Fig. 8a. We note that after a brief control transient, the control agent navigates the NODE-ROM to an equilibrium(steady) state and stabilizes it. The quantities targeted for minimization, D and P_f, estimated from the predicted trajectory $u(t)$, are shown in Figure 8c, revealing that this equilibrium exhibits dissipation much lower than the natural unactuated dynamics. To

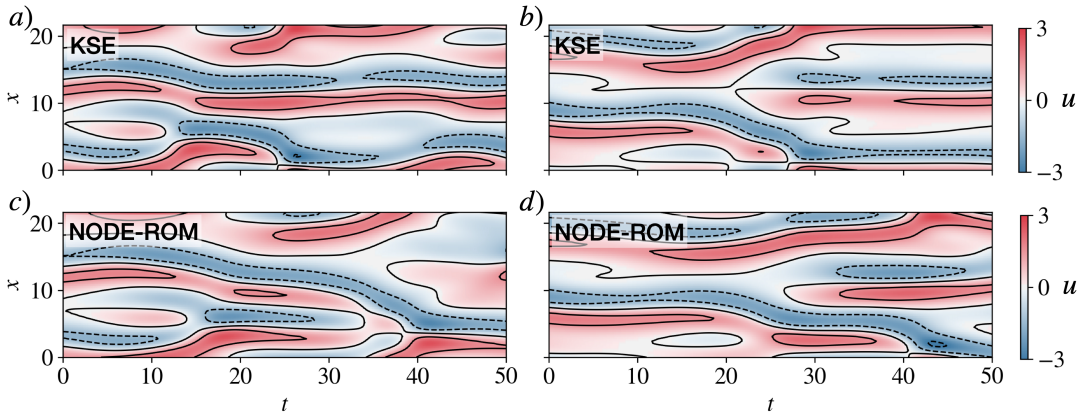

FIG. 7: Example unactuated trajectories of the KSE in a) and b) and their corresponding decoded NODE-ROM ($d_h = 12$) forecasts starting from the same initial conditions in c) and d), respectively.

assess how well this DManD-RL control policy transfers to the original KSE (i.e. the true system), the same policy is applied to the true KSE with the same initial condition, as shown in Fig. 8b. We note that the controlled trajectory in the KSE yields not only quantitatively similar transient behavior but also the same low-dissipation equilibrium state as was targeted in the NODE-ROM. The transient behaviors between the two are structurally very similar, although the NODE-ROM displays slightly less strongly damped oscillations as it drives the trajectory to the steady state. The values of D and P_f computed from the true system, shown in Fig. 8d, are nearly identical to that of the NODE-ROM in Fig. 8c.

To demonstrate the robustness of the DManD-RL policy, shown in Fig. 8e are the dissipation trajectories of the true KSE beginning from 15 randomly sampled test initial conditions that the DManD-RL control agent has not seen before. We highlight that the control agent is able to consistently navigate the system to the same low-dissipation state within ~ 150 time units, with one initial condition requiring ~ 200 time units to converge. Finally we note that although the RL training horizons were only 100 time units long, the control agent is able to generalize to achieve and maintain control well beyond the the horizon it was trained in.

Here we emphasize that the DManD-RL policy drives the dynamics to an equilibrium state in both the NODE-ROM and the true KSE, indicating that not only does the NODE-ROM capture this state, but it captures the dynamics leading to it accurately enough such

that the RL agent could discover it during training and exploit it in a manner that still translates to the original system. We further emphasize that both the NODE-ROM and agent were never explicitly informed of this low-dissipation state's existence. Finally, we highlight that the discovered low-dissipation state is an unstable state that is stabilized by the control agent. If control is removed, the system returns to the natural chaotic dynamics.

These observations indicate that the RL policy trained on the model transfers very well to the true system. We attribute this performance to the fact that both the NODE-ROM and RL agent operate in Markovian fashion, i.e. even if the model has slight inaccuracies, so long as the modeled dynamics are reasonably accurate this does not matter once the agent makes its new state observation.

Returning to the dynamical significance of the low-dissipation equilibrium state discovered and stabilized by the RL agent, a continuation in mean forcing magnitude was performed. To do so, we Newton-solved for equilibrium solutions to the KSE starting with the discovered equilibrium state while gradually decreasing the magnitude of the mean actuation profile to zero, as was done in [12]. Solutions identified by this continuation in forcing magnitude are shown in Fig. 10, which reveals that equilibrium state captured by the NODE-ROM and discovered by the RL agent is connected to a known existing solution of the KSE known as $E1$ [46]; we obtained a similar result with an RL agent trained on interactions with the full system [12]. A similar observation was made for RL control of 2D bluff body flow [9]. We speculate that in systems with complex nonlinear dynamics, the discovery and stabilization of desirable underlying equilibrium solutions (or other recurrent saddle-point solutions such as unstable periodic orbits) of the system may be a fairly general feature of RL flow control approaches. The nonlinear and exploratory nature of RL algorithms facilitates the discovery of such solutions, and since the dynamics are slow near these solutions, little control action should be required to keep trajectories near them.

We speculate that in systems with complex dynamics, the discovery and stabilization of desirable underlying solutions of the system may be a fairly general feature of RL flow control approaches that aim to minimize dissipation while penalizing control action – ; as was shown with the KSE in [12] and bluff-body flows in [9]. This is a promising outlook for RL as the dynamics of even more complex chaotic systems, such as turbulent flows governed by the Navier-Stokes equations, are also known to be structured around such solutions [51].

To highlight the importance of the type of data-driven model, we compare to Dynamic Mode Decomposition (DMD), a common data-driven method that has been applied to fluid flows and dynamical systems. Recently, Qin et al. [52] demonstrated active flow control of 2D cylinder flow with a reward signal targeting the minimization of DMD mode amplitudes. Here we specifically investigate the performance of using DMDc [53], the extension of DMD to account for control input, as an alternate data-driven model of the KSE dynamics for RL policy learning. The DMDc model takes the following form,

$$s_{t+\tau} = \mathbf{A}s_t + \mathbf{B}a_t, \tag{6}$$

where $\mathbf{A}$ is the state transition matrix and $\mathbf{B}$ is the control input matrix. Using the same training data as our NODE-ROM, $[s_t, a_t, s_{t+\tau}]$, , we obtained a full state DMDc model by simultaneously fitting the two matrices with the $[s_t, a_t, s_{t+\tau}]$ data as described in [53]. This model was then used as the environment for the RL policy training.

Shown in Fig. 9a is the DMDc-based RL control agent applied to the DMDc model it was trained in. We show in Fig. 9c that the agent is able to rapidly minimize the DMDc model values of D, P_f. We highlight that the DMDc-based strategy accomplishes this by exploiting the unphysical dynamics of the DMDc model. To elaborate, shown in Fig. 9b is the same strategy applied to the true KSE with the same initial condition as the DMDc trajectory in Fig. 9a. The DMDc-based RL strategy fails to minimize the control objective when applied to the true KSE. Furthermore, the strategy even results in performance that is even worse than the time-averaged uncontrolled system, which can be seen in the above average D, P_f values at long times in Fig. 9d, where the controller appears to get trapped in a high energy region of the KSE. This mismatch in performance is due to the inability of the linear model to describe the nonlinear dynamics of the KSE.

IV. CONCLUSIONS

In this paper we introduce our NODE-ROM-Based RL method, DManD-RL, that maintains an end-to-end data-driven method of learning control policies from a limited data set. The governing equations and control term do not need to be known or specified–we only assume that the system's actuated dynamics can be represented by some governing system

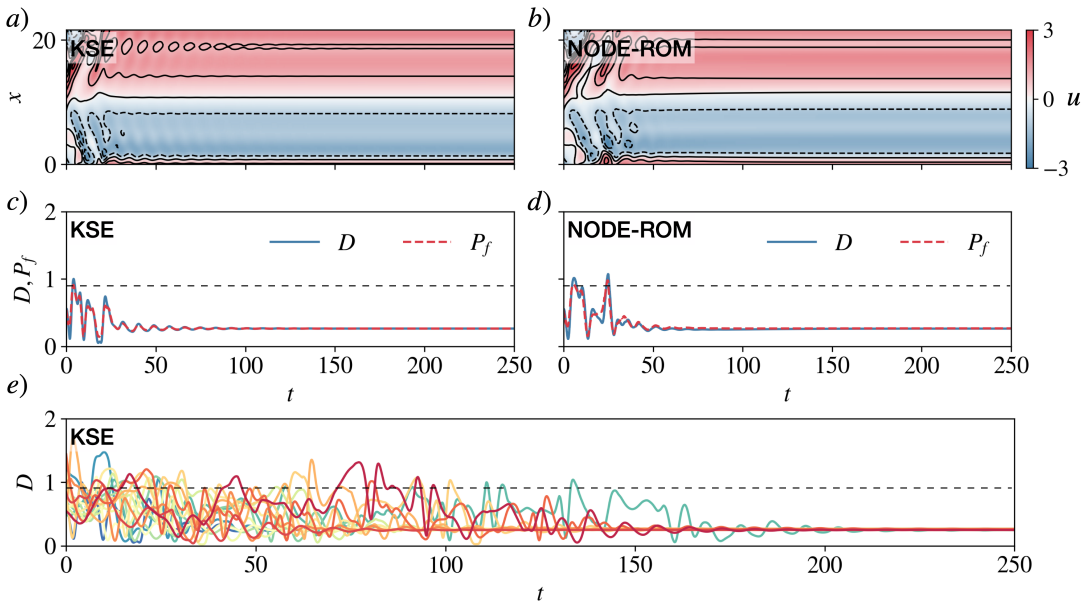

FIG. 8: ROM-based RL agent applied to the same initial condition in the a) true KSE and b) data-driven reduced-order model (decoded, $d_h = 12$). The corresponding invariant quantities of dissipation and total input power for the c) true KSE and d) learned reduced-order model. The dashed black line represents the system average of the natural KSE dynamics. e) Controlled dissipation trajectories of the true KSE beginning from 15 randomly sampled test initial conditions of the KSE.

of ODEs in the manifold coordinate. Furthermore, we do not impose any structural relationship between the control input and the dynamics of the systems as previous methods have done in the past. This is advantageous for many complex flow control systems as the relationship between the dynamics and the control inputs are not simple linear relationships [44, 45]. We exploit the notion that many nominally high-dimensional systems actually display low-dimensional dynamics and aim to capture and model these actuated dynamics from data using a combination of autoencoders and Neural ODEs. Then, with deep RL, we extract control policies from our data-driven ROMs. Importantly, our method does not require RL to directly interact with the target system nor does it require great modification of standard RL algorithms.

Our method identifies the lower-dimensional manifold the actuated dynamics live on with autoencoders and models the dynamics with neural ODEs, which are capable of making predictions for arbitrary time intervals [41] and have been demonstrated to produce good

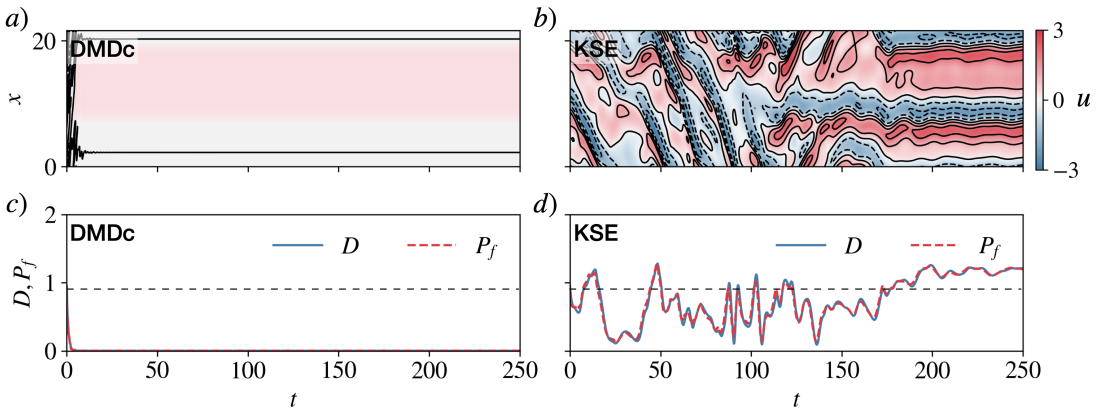

FIG. 9: DMDc control policy applied to the same initial condition in the (a) DMDc model and (b) True KSE. Corresponding dissipation and total input power for the (c) DMDc model and (d) KSE. The dashed black line represents the average of the natural KSE dynamics.

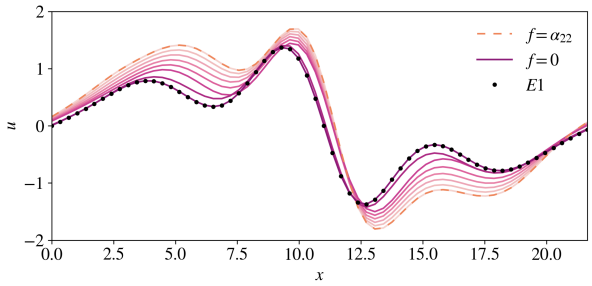

FIG. 10: Forcing continuation from the forced equilibrium state (under forcing $f = \alpha_{22}$) discovered by NODE-ROM based RL policy (orange, dashed) to the unactuated KSE system (purple). The known equilibrium E1 of the KSE system is also provided (dots).

predictions of spatiotemporal chaotic systems [22]. Neural ODEs are also a natural formulation and deep architecture for the systems we are attempting to model and control. Our method also respects the Markovian nature underlying many RL frameworks as well as those of our target dynamical systems, unlike other common data-driven methods such as reservoir computing and recurrent neural networks. The use of high-fidelity low-dimensional models allows for faster interaction simulations (or even running multiple surrogate environments in parallel) compared to costly simulations or experiments.

By using a more informative and compact state space representation than a high-

dimensional sensed state, the RL policy training load is lessened. In naive applications of RL, a portion of the agent's network capacity are exhausted in learning to transform the raw inputs to more useful internal representations [14]. Similar to Ha and Schmidhuber [14], in our method we also explicitly separate the agent's learning of the control policy and the task of learning a useful state representation into two discrete tasks.

We apply our DManD-RL RL method to the KSE, a proxy system for turbulent flows that exhibits rich spatiotemporal chaotic dynamics. From a limited data set generated from trajectories of the KSE under random actuations, we are able to find a reduced-order mapping between the full state and the reduced low-order dynamics of the actuated KSE, as well as to successfully model the dynamics in this reduced space. We find that our NODE-ROM has good forecasting ability and captures ensemble characteristics of the KSE well for not only actuated predictions, but also unactuated predictions, for which it was not given training data. In this work it was found that NODE-ROM training data obtained from snapshots of the KSE experiencing random jet actuations was sufficient. With even more complex systems, it may be possible that this sampling approach is insufficient. If necessary, the NODE-ROM can be iteratively improved by applying the learned control strategy to the true system, collecting additional data, and fine-tuning the NODE-ROM with the new data. Using the updated NODE-ROM, the RL agent can then be updated. Together the control agent and model can be improved in a cyclic training fashion. Finally, we highlight that our model could be alternatively trained and used in the "Dyna"-style [19] for improved online learning.

Utilizing this NODE-ROM in place of the environment, the RL agent is able to discover a low-dissipation equilibrium state and learns to exploit it to minimize D, P_f. When the DManD-RL control policy is deployed to the true KSE, we observe that not only are the same equilibrium states targeted, but the performance is nearly indistinguishable from our learned NODE-ROM. This indicates that not only does the NODE-ROM capture the existence of the forced equilibrium, but it also captures the dynamics sufficiently well such that the agent could find it during training and exploit it in a manner that still translates in the original system. We emphasize that we accomplished this with a 12-dimensional NODE-ROM while the full state is 64- dimensional. A continuation in the magnitude of the forcing profile reveals that the RL discovered equilibrium state is connected to an existing equilibrium solution of

natural KSE. The naturally occurring RL optimization about underlying solutions of the system has been observed in the KSE [12] as well as bluff-body flows [9], which is promising, as more complex dissipative systems, such as the turbulent dynamics of the Navier-Stokes equations, are also known to be organized about various types of invariant solutions [51].

---

[1] David Silver, Aja Huang, Chris J. Maddison, Arthur Guez, Laurent Sifre, George Van Den Driessche, Julian Schrittwieser, Ioannis Antonoglou, Veda Panneershelvam, Marc Lanctot, Sander Dieleman, Dominik Grewe, John Nham, Nal Kalchbrenner, Ilya Sutskever, Timothy Lillicrap, Madeleine Leach, Koray Kavukcuoglu, Thore Graepel, and Demis Hassabis. Mastering the game of Go with deep neural networks and tree search. *Nature*, 529(7587):484–489, 2016. ISSN 14764687. doi:10.1038/nature16961. URL http://dx.doi.org/10.1038/nature16961.

[2] OpenAI, Christopher Berner, Greg Brockman, Brooke Chan, Vicki Cheung, Przemysław Psyho Dębiak, Christy Dennison, David Farhi, Quirin Fischer, Shariq Hashme, Chris Hesse, Rafal Józefowicz, Scott Gray, Catherine Olsson, Jakub Pachocki, Michael Petrov, Henrique Pondé, De Oliveira Pinto, Jonathan Raiman, Tim Salimans, Jeremy Schlatter, Jonas Schneider, Szymon Sidor, Ilya Sutskever, Jie Tang, Filip Wolski, and Susan Zhang. Dota 2 with Large Scale Deep Reinforcement Learning. *ArXiv Preprint*, 2019.

[3] Oriol Vinyals, Igor Babuschkin, Wojciech M. Czarnecki, Michaël Mathieu, Andrew Dudzik, Junyoung Chung, David H. Choi, Richard Powell, Timo Ewalds, Petko Georgiev, Junhyuk Oh, Dan Horgan, Manuel Kroiss, Ivo Danihelka, Aja Huang, Laurent Sifre, Trevor Cai, John P. Agapiou, Max Jaderberg, Alexander S. Vezhnevets, Rémi Leblond, Tobias Pohlen, Valentin Dalibard, David Budden, Yury Sulsky, James Molloy, Tom L. Paine, Caglar Gulcehre, Ziyu Wang, Tobias Pfaff, Yuhuai Wu, Roman Ring, Dani Yogatama, Dario Wünsch, Katrina McKinney, Oliver Smith, Tom Schaul, Timothy Lillicrap, Koray Kavukcuoglu, Demis Hassabis, Chris Apps, and David Silver. Grandmaster level in StarCraft II using multi-agent reinforcement learning. *Nature*, 575(7782):350–354, 2019. ISSN 14764687. doi:10.1038/s41586-019-1724-z. URL http://dx.doi.org/10.1038/s41586-019-1724-z.

[4] David Silver, Thomas Hubert, Julian Schrittwieser, Ioannis Antonoglou, Matthew Lai, Arthur Guez, Marc Lanctot, Laurent Sifre, Dharshan Kumaran, Thore Graepel, Timothy Lilli-

crap, Karen Simonyan, and Demis Hassabis. A general reinforcement learning algorithm that masters chess, shogi, and Go through self-play. *Science*, 362(6419):1140–1144, 2018. doi:10.1126/science.aar6404. URL https://www.science.org/doi/abs/10.1126/science.aar6404.

[5] Jean Rabault, Miroslav Kuchta, Atle Jensen, Ulysse Réglade, and Nicolas Cerardi. Artificial neural networks trained through deep reinforcement learning discover control strategies for active flow control. *Journal of Fluid Mechanics*, 865:281–302, 2019. doi:10.1017/jfm.2019.62.

[6] Dixia Fan, Liu Yang, Zhicheng Wang, Michael S. Triantafyllou, and George Em Karniadakis. Reinforcement learning for bluff body active flow control in experiments and simulations. *Proceedings of the National Academy of Sciences*, 117(42):26091–26098, 2020. ISSN 0027-8424. doi:10.1073/pnas.2004939117. URL https://www.pnas.org/content/117/42/26091.

[7] Feng Ren, Jean Rabault, and Hui Tang. Applying deep reinforcement learning to active flow control in weakly turbulent conditions. *Physics of Fluids*, 33(3):037121, 2021. doi:10.1063/5.0037371. URL https://doi.org/10.1063/5.0037371.

[8] Romain Paris, Samir Beneddine, and Julien Dandois. Robust flow control and optimal sensor placement using deep reinforcement learning. *Journal of Fluid Mechanics*, 913:A25, 2021. doi:10.1017/jfm.2020.1170.

[9] Jichao Li and Mengqi Zhang. Reinforcement-learning-based control of confined cylinder wakes with stability analyses. *Journal of Fluid Mechanics*, 932:A44, 2022. doi:10.1017/jfm.2021.1045.

[10] Gerben Beintema, Alessandro Corbetta, Luca Biferale, and Federico Toschi. Controlling Rayleigh–Bénard convection via reinforcement learning. *Journal of Turbulence*, 21(9-10):585–605, 2020. doi:10.1080/14685248.2020.1797059. URL https://doi.org/10.1080/14685248.2020.1797059.

[11] M. A. Bucci, O. Semeraro, A. Allauzen, G. Wisniewski, L. Cordier, and L. Mathelin. Control of chaotic systems by deep reinforcement learning. *Proceedings of the Royal Society A: Mathematical, Physical and Engineering Sciences*, 475(2231):20190351, 2019. doi:10.1098/rspa.2019.0351. URL https://royalsocietypublishing.org/doi/abs/10.1098/rspa.2019.0351.

[12] Kevin Zeng and Michael D. Graham. Symmetry reduction for deep reinforcement learning active control of chaotic spatiotemporal dynamics. *Phys. Rev. E*, 104:014210, Jul 2021. doi:

10.1103/PhysRevE.104.014210. URL https://link.aps.org/doi/10.1103/PhysRevE.104.014210.

[13] Simon S. Du, Sham M. Kakade, Ruosong Wang, and Lin F. Yang. Is a Good Representation Sufficient for Sample Efficient Reinforcement Learning? In *8th International Conference on Learning Representations, ICLR 2020, Addis Ababa, Ethiopia, April 26-30, 2020*. OpenReview.net, 2020. URL https://openreview.net/forum?id=r1genAVKPB.

[14] David Ha and Jürgen Schmidhuber. Recurrent World Models Facilitate Policy Evolution. In Samy Bengio, Hanna M. Wallach, Hugo Larochelle, Kristen Grauman, Nicolò Cesa-Bianchi, and Roman Garnett, editors, *Advances in Neural Information Processing Systems 31: Annual Conference on Neural Information Processing Systems 2018, NeurIPS 2018, December 3-8, 2018, Montréal, Canada*, pages 2455–2467, 2018. URL https://proceedings.neurips.cc/paper/2018/hash/2de5d16682c3c35007e4e92982f1a2ba-Abstract.html.

[15] Anusha Nagabandi, Gregory Kahn, Ronald S. Fearing, and Sergey Levine. Neural Network Dynamics for Model-Based Deep Reinforcement Learning with Model-Free Fine-Tuning. In *2018 IEEE International Conference on Robotics and Automation, ICRA 2018, Brisbane, Australia, May 21-25, 2018*, pages 7559–7566. IEEE, 2018. doi:10.1109/ICRA.2018.8463189. URL https://doi.org/10.1109/ICRA.2018.8463189.

[16] Niklas Wahlström, Thomas B. Schön, and Marc Peter Deisenroth. From Pixels to Torques: Policy Learning with Deep Dynamical Models. *arXiv*, abs/1502.02251, 2015. URL http://arxiv.org/abs/1502.02251.

[17] Manuel Watter, Jost Tobias Springenberg, Joschka Boedecker, and Martin A. Riedmiller. Embed to Control: A Locally Linear Latent Dynamics Model for Control from Raw Images. In Corinna Cortes, Neil D. Lawrence, Daniel D. Lee, Masashi Sugiyama, and Roman Garnett, editors, *Advances in Neural Information Processing Systems 28: Annual Conference on Neural Information Processing Systems 2015, December 7-12, 2015, Montreal, Quebec, Canada*, pages 2746–2754, 2015. URL https://proceedings.neurips.cc/paper/2015/hash/a1afc58c6ca9540d057299ec3016d726-Abstract.html.

[18] Vladimir Feinberg, Alvin Wan, Ion Stoica, Michael I. Jordan, Joseph E. Gonzalez, and Sergey Levine. Model-Based Value Estimation for Efficient Model-Free Reinforcement Learning. *arXiv*, abs/1803.00101, 2018. URL http://arxiv.org/abs/1803.00101.

[19] Richard S. Sutton and Andrew G. Barto. *Reinforcement Learning: An Introduction, Second Edition*. MIT Press, 2018.

[20] Xin-Yang Liu and Jian-Xun Wang. Physics-informed Dyna-style model-based deep reinforcement learning for dynamic control. *Proceedings of the Royal Society A: Mathematical, Physical and Engineering Sciences*, 477(2255):20210618, 2021. doi:10.1098/rspa.2021.0618. URL https://royalsocietypublishing.org/doi/abs/10.1098/rspa.2021.0618.

[21] Sean Meyn. *Control Systems and Reinforcement Learning*. Cambridge University Press, 2022.

[22] Alec J. Linot and Michael D. Graham. Data-Driven Reduced-Order Modeling of Spatiotemporal Chaos with Neural Ordinary Differential Equations. *arXiv*, abs/2109.00060, 2021. URL https://arxiv.org/abs/2109.00060.

[23] Philip Holmes, John L. Lumley, Gahl Berkooz, and Clarence W. Rowley. *Galerkin projection*, pages 106–129. Cambridge Monographs on Mechanics. Cambridge University Press, 2 edition, 2012. doi:10.1017/CBO9780511919701.006.

[24] M. Marion and R. Temam. Nonlinear Galerkin methods: The finite elements case. *Numerische Mathematik*, 57(1):205–226, 1990. ISSN 0029599X. doi:10.1007/BF01386407.

[25] F. Jauberteau, C. Rosier, and R. Temam. The nonlinear Galerkin method in computational fluid dynamics. *Applied Numerical Mathematics*, 6(5):361–370, 1990. ISSN 01689274. doi: 10.1016/0168-9274(90)90026-C.

[26] M D Graham, R H Steen, and E S Titi. Nonlinear Science Computational Efficiency and Approximate Inertial. *New York*, 3:153–167, 1993.

[27] Bosco García-Archilla, Julia Novo, and Edriss S. Titi. Postprocessing the Galerkin Method: a Novel Approach to Approximate Inertial Manifolds. *SIAM Journal on Numerical Analysis*, 35(3):941–972, 1998. doi:10.1137/S0036142995296096. URL https://doi.org/10.1137/S0036142995296096.

[28] Zhong Yi Wan, Pantelis Vlachas, Petros Koumoutsakos, and Themistoklis Sapsis. Data-assisted reduced-order modeling of extreme events in complex dynamical systems. *PLoS ONE*, 13(5):1–22, 2018. ISSN 19326203. doi:10.1371/journal.pone.0197704.

[29] M. Raissi, P. Perdikaris, and G.E. Karniadakis. Physics-informed neural networks: A deep learning framework for solving forward and inverse problems involving nonlinear partial differential equations. *Journal of Computational Physics*, 378:686–707, 2019. ISSN 0021-

9991. doi:https://doi.org/10.1016/j.jcp.2018.10.045. URL https://www.sciencedirect.com/science/article/pii/S0021999118307125.

[30] J. Nathan Kutz, Steven L. Brunton, Bingni W. Brunton, and Joshua L. Proctor. *Dynamic Mode Decomposition*. Society for Industrial and Applied Mathematics, Philadelphia, PA, 2016. doi:10.1137/1.9781611974508. URL https://epubs.siam.org/doi/abs/10.1137/1.9781611974508.

[31] Andrzej Lasota and Michael C Mackey. *Chaos, Fractals and Noise: stochastic aspects of dynamics*. Springer. Springer, New York, second edition, 1994. doi:10.1007/978-1-4612-4286-4.

[32] Marko Budišić, Ryan Mohr, and Igor Mezić. Applied Koopmanism. *Chaos: An Interdisciplinary Journal of Nonlinear Science*, 22(4):047510, 2012. doi:10.1063/1.4772195. URL https://doi.org/10.1063/1.4772195.

[33] J J Hopfield. Neural networks and physical systems with emergent collective computational abilities. *Proceedings of the National Academy of Sciences*, 79(8):2554–2558, 1982. ISSN 0027-8424. doi:10.1073/pnas.79.8.2554. URL https://www.pnas.org/content/79/8/2554.

[34] Sepp Hochreiter and Jürgen Schmidhuber. Long Short-Term Memory. *Neural Computation*, 9(8):1735–1780, 11 1997. ISSN 0899-7667. doi:10.1162/neco.1997.9.8.1735. URL https://doi.org/10.1162/neco.1997.9.8.1735.

[35] H. Jaeger. The "echo state" approach to analysing and training recurrent neural networks. GMD Report 148, GMD - German National Research Institute for Computer Science, 2001. URL http://www.faculty.jacobs-university.de/hjaeger/pubs/EchoStatesTechRep.pdf.

[36] Robert Legenstein and Wolfgang Maass. Edge of chaos and prediction of computational performance for neural circuit models. *Neural Networks*, 20(3):323–334, 2007. ISSN 0893-6080. doi:https://doi.org/10.1016/j.neunet.2007.04.017. URL https://www.sciencedirect.com/science/article/pii/S0893608007000433. Echo State Networks and Liquid State Machines.

[37] Junyoung Chung, Caglar Gulcehre, Kyunghyun Cho, and Yoshua Bengio. Empirical evaluation of gated recurrent neural networks on sequence modeling. In *NIPS 2014 Workshop on Deep Learning, December 2014*, 2014.

[38] P.R. Vlachas, J. Pathak, B.R. Hunt, T.P. Sapsis, M. Girvan, E. Ott, and P. Koumoutsakos. Backpropagation algorithms and Reservoir Computing in Recurrent Neural Networks for the forecasting of complex spatiotemporal dynamics. *Neural Networks*, 126: 191–217, 2020. ISSN 0893-6080. doi:https://doi.org/10.1016/j.neunet.2020.02.016. URL https://www.sciencedirect.com/science/article/pii/S0893608020300708.

[39] Steven L. Brunton, Joshua L. Proctor, and J. Nathan Kutz. Discovering governing equations from data by sparse identification of nonlinear dynamical systems. *Proceedings of the National Academy of Sciences*, 113(15):3932–3937, 2016. ISSN 0027-8424. doi:10.1073/pnas.1517384113. URL https://www.pnas.org/content/113/15/3932.

[40] R. Gonzalez-Garcia, R. Rico-Martinez, and I. G. Kevrekidis. Identification of distributed parameter systems: A neural net based approach. *Computers & Chemical EngineeringComputers & Chemical Engineering*, 22:S965–S968, 1998.

[41] Tian Qi Chen, Yulia Rubanova, Jesse Bettencourt, and David Duvenaud. Neural Ordinary Differential Equations. In Samy Bengio, Hanna M. Wallach, Hugo Larochelle, Kristen Grauman, Nicolò Cesa-Bianchi, and Roman Garnett, editors, *Advances in Neural Information Processing Systems 31: Annual Conference on Neural Information Processing Systems 2018, NeurIPS 2018, December 3-8, 2018, Montréal, Canada*, pages 6572–6583, 2018. URL https://proceedings.neurips.cc/paper/2018/hash/69386f6bb1dfed68692a24c8686939b9-Abstract.html.

[42] Roger Temam. *Infinite-Dimensional Dynamical Systems in Mechanics and Physics*. Springer, New York, NY, 1977.

[43] Alec J. Linot and Michael D. Graham. Deep learning to discover and predict dynamics on an inertial manifold. *Phys. Rev. E*, 101:062209, Jun 2020. doi:10.1103/PhysRevE.101.062209. URL https://link.aps.org/doi/10.1103/PhysRevE.101.062209.

[44] Jovan D. Boskovic, Lingji Chen, and Raman K. Mehra. Adaptive Control Design for Nonaffine Models Arising in Flight Control. *Journal of Guidance, Control, and Dynamics*, 27(2):209–217, 2004. doi:10.2514/1.1106. URL https://doi.org/10.2514/1.1106.

[45] Behdad Geranmehr and Saeed Rafee Nekoo. Nonlinear suboptimal control of fully coupled non-affine six-DOF autonomous underwater vehicle using the state-dependent Riccati equation. *Ocean Engineering*, 96:248–257, 2015. ISSN 0029-8018. doi:

https://doi.org/10.1016/j.oceaneng.2014.12.032. URL https://www.sciencedirect.com/science/article/pii/S0029801814004892.

[46] Predrag Cvitanovic, Ruslan L. Davidchack, and Evangelos Siminos. On the State Space Geometry of the Kuramoto-Sivashinsky Flow in a Periodic Domain. *SIAM J. Appl. Dyn. Syst.*, 9(1):1–33, 2010. doi:10.1137/070705623. URL https://doi.org/10.1137/070705623.

[47] Ian Goodfellow, Yoshua Bengio, and Aaron Courville. *Deep Learning*. MIT Press, 2016. http://www.deeplearningbook.org.

[48] J.R. Dormand and P.J. Prince. A family of embedded Runge-Kutta formulae. *Journal of Computational and Applied Mathematics*, 6(1):19–26, 1980. ISSN 0377-0427. doi: https://doi.org/10.1016/0771-050X(80)90013-3. URL https://www.sciencedirect.com/science/article/pii/0771050X80900133.

[49] Timothy P. Lillicrap, Jonathan J. Hunt, Alexander Pritzel, Nicolas Heess, Tom Erez, Yuval Tassa, David Silver, and Daan Wierstra. Continuous control with deep reinforcement learning, 2019.

[50] X. Ding, H. Chaté, P. Cvitanović, E. Siminos, and K. A. Takeuchi. Estimating the Dimension of an Inertial Manifold from Unstable Periodic Orbits. *Phys. Rev. Lett.*, 117:024101, Jul 2016. doi:10.1103/PhysRevLett.117.024101. URL https://link.aps.org/doi/10.1103/PhysRevLett.117.024101.

[51] Michael D. Graham and Daniel Floryan. Exact Coherent States and the Nonlinear Dynamics of Wall-Bounded Turbulent Flows. *Annual Review of Fluid Mechanics*, 53(1):227–253, 2021. doi:10.1146/annurev-fluid-051820-020223. URL https://doi.org/10.1146/annurev-fluid-051820-020223.

[52] Sheng Qin, Shuyue Wang, Jean Rabault, and Gang Sun. An application of data driven reward of deep reinforcement learning by dynamic mode decomposition in active flow control. *ArXiv Preprint*, 2021.

[53] Joshua L. Proctor, Steven L. Brunton, and J. Nathan Kutz. Dynamic Mode Decomposition with Control. *SIAM Journal on Applied Dynamical Systems*, 15(1):142–161, 2016. doi: 10.1137/15M1013857. URL https://doi.org/10.1137/15M1013857.